Lawrence Berkeley National Laboratory
LBL Publications

Title
Electrode Lithiation: Effects of Particle Size, Electronic Connectivity, and Incoherent Nanoscale Domains on the Sequence of Lithiation in LiFePO4 Porous Electrodes (Adv. Mater. 42/2015)

Permalink

Journal
Advanced Materials, 27(42)

ISSN
0935-9648

Authors
Li, Yiyang
Meyer, Sophie
Lim, Jongwoo
et al.

Publication Date
2015-11-01

DOI
10.1002/adma.201570286

Peer reviewed

Effects of Particle Size, Electronic Connectivity, and Incoherent Nanoscale Domains on the Sequence of Lithiation in LiFePO₄ Porous Electrodes

Yiyang Li, Sophie Meyer, Jongwoo Lim, Sang Chul Lee, William E. Gent, Stefano Marchesini, Harinarayan Krishnan, Tolek Tyliszczak, David Shapiro, Arthur L. David Kilcoyne, and William C. Chueh*

Lithium iron phosphate ($LiFePO_4$) is a promising positive battery electrode material and a model system for studying Li intercalation.[1,2] In porous battery electrodes containing an ensemble of particles, the sequence of lithiation, that is whether or not a given particle lithiates before another, is an important indicator of the thermodynamics and kinetics of ion insertion. The position and size dependence of this sequence, in particular, give information about the loss mechanisms and rate-limiting processes, and have been used to engineer materials for batteries,[3,4] catalysis,[5] hydrogen storage,[6] and memristors.[7] In this work, we combine synchrotron-based scanning transmission X-ray microscopy (STXM) and ptychography with transmission electron microscopy (TEM) to determine the sequence of lithiation in $LiFePO_4$ electrodes by measuring the single-particle state-of-charge (SOC) for ≈800 $LiFePO_4$ particles in partially discharged electrodes. Through correlating this sequence to the size of the particles in the electrode, we show that variations in the local electronic connectivity within the carbon black network play a critical role in determining the sequence of lithiation in these electrodes. Additionally, by controlling for and disentangling the effects of the local electronic connectivity, we capture the intrinsic particle size dependence of the sequence of lithiation.

Y. Li, Dr. J. Lim, Dr. S. C. Lee, Prof. W. C. Chueh
Department of Materials Science and Engineering
Stanford University
496 Lomita Mall, Stanford, CA 94305, USA
E-mail: wchueh@stanford.edu
S. Meyer
Department of Physics
Stanford University
382 Via Pueblo Mall, Stanford, CA 94305, USA
W. E. Gent
Department of Chemistry
Stanford University
Stanford, CA 94305, USA
Dr. S. Marchesini, Dr. H. Krishnan, Dr. T. Tyliszczak,
Dr. D. Shapiro, Dr. A. L. D. Kilcoyne
Advanced Light Source One Cyclotron Road
Lawrence Berkeley National Laboratory
Berkeley, CA 94720, USA
Prof. W. C. Chueh
Stanford Institute of Materials and Energy Sciences
SLAC National Accelerator Laboratory
2575 Sand Hill Road, Menlo Park, CA 94025, USA

There have been several reports on the sequence of lithiation in $LiFePO_4$ porous electrodes, providing insights into the macroscopic transport gradients (on the length scale of tens of microns) as well as on the microscopic particle size dependence of lithiation (on the length scale of tens to hundreds of nanometers).[8–18] In electrodes thicker than ≈100 μm, particles closer to the counter electrode lithiate preferentially, reflecting ion transport limitations in the electrolyte.[10,15,16] In thinner electrodes, on the other hand, lithiation proceeds uniformly on the macroscopic length scale and exhibits negligible dependence on the distance from the counter electrode.[9,14] While the macroscopic sequence of lithiation in the porous electrode is well understood, the sequence of lithiation on the single-particle length scale is not, particularly regarding the particle size dependence. Report range from negligible size dependence[9] to a preference to lithiate smaller particles.[10] Additionally, it was recently shown that smaller particles are less likely to crack than larger ones,[18,19] but it is unclear how mechanical failure affects the sequence of lithiation.

Different models have been proposed to describe the sequence of lithiation in $LiFePO_4$ electrodes. It is generally accepted that resistive electronic and ionic wiring in the carbon network and/or the electrolyte within the porous electrode create the macroscopic lithiation front.[10,15,16,20,21] Particle-to-particle variations in the wiring have been suggested theoretically to cause some particles to lithiate before others, although the dependence of this effect on particle size is not clear.[14,22] Most kinetic and thermodynamic models predict that smaller particles preferentially lithiate because they have higher surface area to volume ratios,[23–26] reduced diffusion lengths,[26–28] and/or narrower miscibility gaps as a result of surface energy and coherency strain.[29–33]

Here, we systematically investigate the sequence of lithiation in $LiFePO_4$ electrodes. We imaged the SOC of ≈800 particles in partially discharged $LiFePO_4$ electrodes (particle size between ≈50 and ≈500 nm) using both STXM and high-resolution ptychography. For an electrode with high carbon black loading, the smaller particles lithiate before the larger ones. In contrast, the sequence of lithiation is nearly independent of particle size for an electrode with a moderate, technologically relevant carbon black loading. We propose that local variations in the electronic connectivity between $LiFePO_4$ and carbon black particles mask the particle size dependence of lithiation, and that the most resistive process in a $LiFePO_4$ electrode is the electronic conduction between the particles' surface and the nearest branch

of the percolated carbon network. We also correlate the intra-particle SOC distribution to the local crystallography by performing TEM on the same particles. Correlative TEM and X-ray ptychography revealed that incoherent, possibly amorphous domains within individual particles, approximately 20 nm in size, lithiate as if they are separate particles.

We fabricated 60 µm thick LiFePO$_4$ electrodes with different carbon black loadings. Electrode "C5" employed a technologically relevant, high mass loading of active material: 89 wt% carbon-coated LiFePO$_4$ (Mitsui Engineering Shipbuilding Co., Ltd), 5 wt% carbon black (Timcal C65), and 6 wt% poly-(vinylidene fluoride) (PVDF) binder. Electrode "C20" contained 74 wt% LiFePO$_4$, 20 wt% carbon black, and 6 wt% PVDF; this electrode exhibits better electronic conduction and sufficient carbon black loading to create a fully percolating electronic network.[34] To minimize macroscopic ion transport gradients, we used dilute electrodes with high porosities, ≈60% and ≈70% for the C5 and C20 electrodes, respectively. The electrodes were assembled into CR2016 coin cells with Li metal anodes and organic liquid electrolytes (1 M LiPF$_6$ in ethylene carbonate/diethyl carbonate/dimethyl carbonate). The specific capacity of each electrode was ≈150 mAh g^{-1} (Figure S1, Supporting Information). Lowering the C20 electrode porosity with a uni-axial press to ≈40% yielded essentially identical electrochemical charging and discharging curves (Figure S2, Supporting Information), confirming that the electrodes are sufficiently dilute to prevent ionic transport limitations, and is further validated using SOC mapping. Figure S3 (Supporting Information) plots the size distribution of the LiFePO$_4$ particles. More details of the experimental methods are available in Supporting Information.

We cycled each coin cell five times at a rate of C/10 for charge and C/5 for discharge (where C indicates the rate to discharge a battery in 1 h); subsequently, we charged them to 100% SOC at C/10, and discharged them to 50% SOC at 2 C. We then rapidly disassembled the cells inside an Ar-filled glove box. The LiFePO$_4$ electrodes were removed, rinsed with excess dimethyl carbonate, and dried under vacuum. The disassembly process was completed within 2 min of stopping the current. By rapidly disassembling the electrode and removing the electrolyte, we minimize interparticle Li transport, as shown in previous work.[9,14] Extracted electrodes were dried and cross-sectioned using a Leica ultramicrotome into ≈200 nm thick slices, which preserved the location of the particles within the porous electrode and minimized overlapping particles.

We imaged these cross-sections using STXM at beam line 5.3.2.2[35] and ptychography[13] at beam line 11.0.2.2[36] at the Advanced Light Source. With a 30 nm step size and an acquisition time of 10 s µm^{-2} per energy, STXM was used to image three 5 µm × 5 µm regions in each electrode, located along the thickness of the electrode. This field of view corresponds to about 400 isolated particles per electrode. Ptychography, or scanning coherent diffractive imaging, enables imaging near the diffraction limit.[13,18,37] We obtain coherent diffractive images with an acquisition time of 600 s µm^{-2} per energy and reconstruct them into real-space images with 5 nm pixels[13] (currently, about 90% of the acquisition time in ptychography results from the time needed to read from the 2D area detector). Ptychography has recently demonstrated 5 nm resolution in 1D and 18 nm resolution chemical composition mapping in 2D.[13] Because

of the longer acquisition time of ptychography compared to STXM, we reduced the imaging area to one 2 µm × 2 µm region inside one of the previously imaged STXM region in each electrode (white squares in **Figure 1**a,b).

We employ a previously validated quantification approach to determine the local SOC,[9,14,38] which is summarized below. We acquire the X-ray absorption spectra (XAS) across the Fe L$_3$ edge at each pixel. To identify the single-pixel SOC, we fit a linear combination of fully charged and fully discharged reference spectra (Figure S5, Supporting Information), acquired from electrochemically cycled electrodes (Figure S6, Supporting Information), to the XAS at every pixel.[9,38] The SOC maps are shown in Figure 1a–d, where red and green pixels indicate fully lithiated (discharged, LiFe^{2+}PO$_4$) and fully delithiated (charged, Fe^{3+}PO$_4$), respectively. After identifying the boundaries of well-isolated particles using bright field (BF) TEM (Figure 1e,f), we use the corresponding STXM map to identify the SOC of each particle. Each particle is categorized as either Li-rich (0–20% SOC), Li-poor (80–100% SOC), or actively discharging (20–80% SOC), following previous work.[14]

We discuss the SOC mapping results in decreasing length scales, starting with the average SOC for each region imaged along the thickness of the porous electrode. A strong lithiation gradient along the electrode was not detected from the average SOC of the 5 µm × 5 µm STXM maps (Figure S7, Supporting Information). This observation implies that electrode-level electronic or ionic transport gradients are weak, a result of the relatively thin and porous electrode films used in this study. As a result, each region is representative of the entire electrode's behavior.

Next, we discuss the single-particle SOCs and their distribution in the porous electrode. Even in the absence of quantitative analysis, Figure 1a–d clearly shows the presence of both Li-rich and Li-poor particles, indicating that most of the particles are either fully discharged or have yet to discharge. From the STXM SOC maps (Figure 1a,b), the active particle fractions for the C5 and C20 electrodes are 14 ± 2% and 12 ± 2%, respectively. From the ptychography SOC maps, they are 11 ± 6% and 7 ± 5%. The error in the latter is larger because of the fewer number of particles imaged (the error was calculated assuming a binomial distribution, active or not active, taken at one standard deviation). These values are consistent with previous work, which show a small active particle fraction at these cycling rates.[8–10,14] Importantly, this result shows that the active particle fraction is not strongly dependent on the carbon black loading in the electrode. Next, turning to the ptychography results, Figure S8 (Supporting Information) shows a correlation plot comparing the single-particle SOCs determined via STXM and via ptychography. The excellent correlation confirms the consistency of the two microscopy methods, with ptychography providing a significantly higher spatial resolution (Figure 1c,d). Ptychography's higher spatial resolution reveals particles that are too small to be observed clearly in STXM, as well as nanoscale domains within particles, a point that we will return to later.

Having quantified the SOC of individual particles, we then assess how the SOC is correlated to the particle size. Specifically, we determine the size of Li-rich and Li-poor particles by measuring the projected Feret dimension using the TEM images of the same region. We bin the particle size into
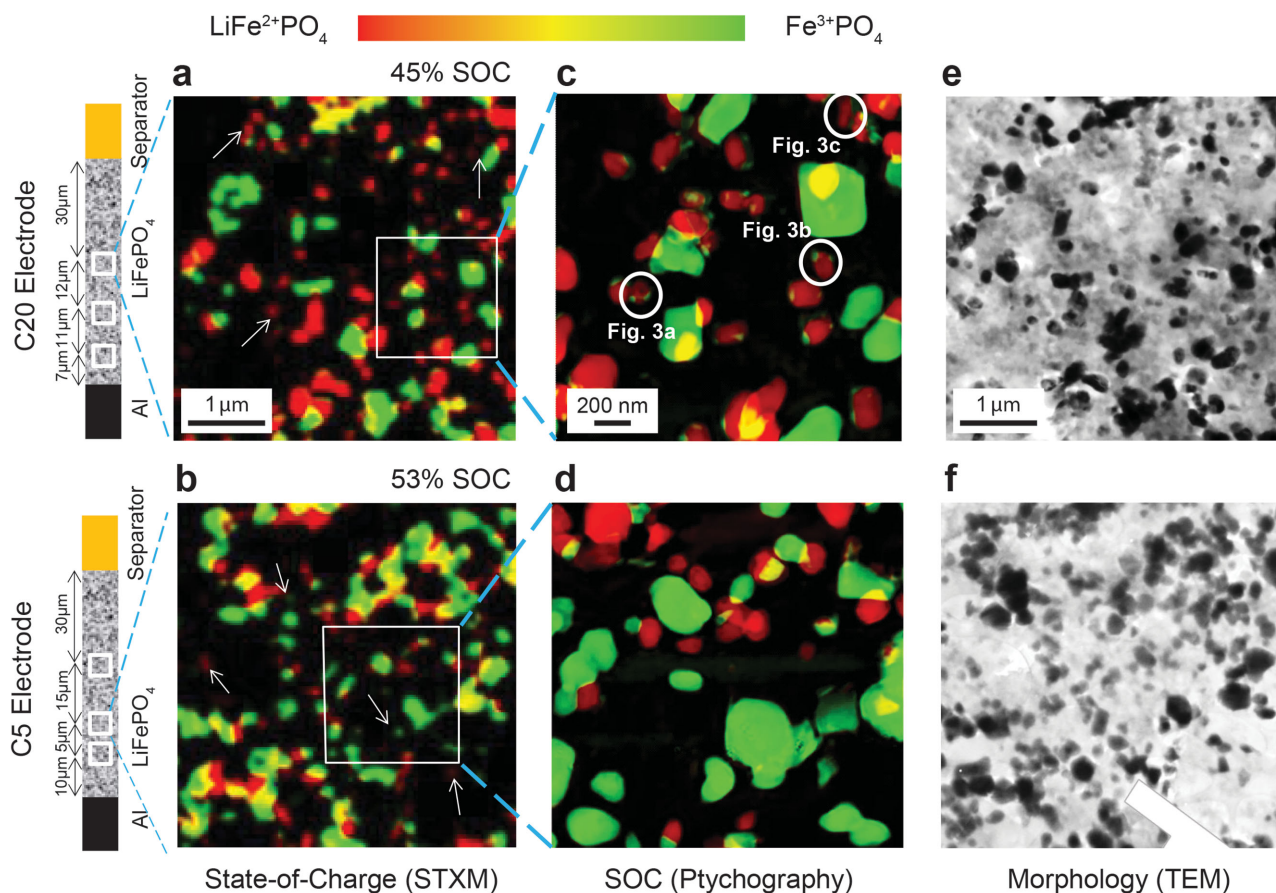
Figure 1. State-of-charge (SOC) maps and morphology images of partially discharged LiFePO₄ electrodes. a,b) STXM of a 5 μm × 5 μm region at 30 nm step size; Figure S4 (Supporting Information) shows the SOC maps for the other imaged regions. The C20 electrode was sectioned from an electrode containing 20 wt% carbon black, and the C5 electrode from an electrode containing 5 wt% carbon black. The hue represents the SOC, while the brightness represents the amount of Fe in that pixel. The mean SOC of each imaged region (45% and 53% SOC) agrees well with the global electrochemical SOC (50%). The white arrows point to some smaller particles. c,d) High-resolution ptychography images of a 2 μm × 2 μm region in each electrode. In Figure 3, we conduct dark field TEM on the particles circled here. e,f) TEM images of the same 5 μm × 5 μm regions in the electrodes.

9 divisions, with each bin having a size range spanning 50 nm. **Figure 2** plots the fraction of Li-rich and Li-poor particles in each bin; active particles are not included in this analysis. In the C20 electrode, the fraction of Li-rich particles decreases with increased particle size, suggesting that the smaller particles lithiate before the larger ones (Figure 2a). For example, $90 \pm 3\%$ of small particles between 100 and 150 nm are Li-rich, whereas only $25 \pm 22\%$ of the large particles between 450 and 500 nm are Li-rich. On the other hand, the C5 electrode exhibits a much weaker size dependence (Figure 2b), indicating that smaller particles are not necessarily more likely to lithiate before larger particles. The dichotomy in the size dependence can be seen directly in Figure 1a,b: smaller particles (white arrows) are nearly all in the Li-rich state in the C20 sample, whereas they are both in the Li-rich and Li-poor states in the C5 sample. Since both electrodes use the same batch of LiFePO₄ particles, the observed differences between the two electrodes cannot arise from variations in the thermodynamics or the surface reactivity between the two samples. Moreover, because electrode-level transport gradients are weak, the size dependence is does not result from macroscopic lithiation gradients.

Finally, we investigate the nanoscale Li-poor domains within otherwise Li-rich particles. The strong SOC gradients make these domains visible in the ptychography maps (Figure 1c), and indicate that different domains in a particle lithiate at different times. These features are as small as 20 nm and only appear in the C20 electrode, and have not been previously observed in STXM due resolution limitations. We conducted dark field (DF) TEM on some of these particles to assess the crystallographic relationship between the domains and the remainder of the particle (**Figure 3**). In the majority of particles characterized, incoherent domains were also visible in the DF images and correspond precisely to the SOC domains (Figure 3a,b). Therefore, these Li-poor domains are crystallographically incoherent with the rest of the particle, which is Li rich. We note that the DF images use a 2 nm⁻¹ objective aperture, which does not identify coherent phase boundaries because the Li-rich triphylite and Li-poor heterosite phases have very similar lattice constants.[1] Some fully lithiated particles also contain incoherent crystal domains (Figure 3c). Nano-sized incoherent domains were not observed in the pristine, as synthesized material, suggesting that they formed during electrochemical cycling.

COMMUNICATION
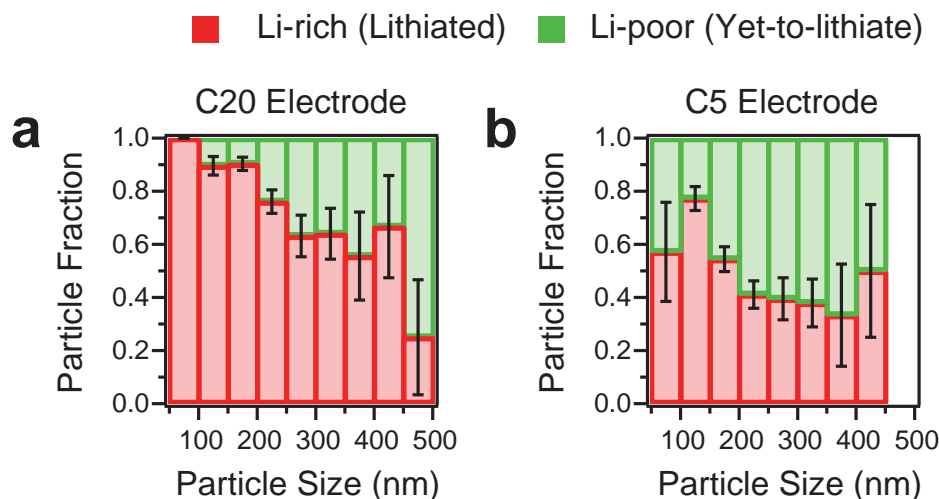
Figure 2. Particle size dependence of the sequence of lithiation. a) The smaller particles preferentially lithiate in the C20 electrode. b) Weak dependence in the C5 electrode. The error bars represent one standard deviation assuming a binomial distribution.

To interpret these incoherent domains, we perform high-resolution TEM (HRTEM) on some cycled LiFePO$_4$ particles dispersed on holey carbon TEM grids; the embedded epoxy precludes HRTEM on the microtomed electrodes. Figure 3d shows the BF image and selected area electron diffraction of a single particle. Diffraction, DF (Figure 3e), and HRTEM (Figure 3f) reveal the presence of two crystal domains. This likely result from two particles sintered together during synthesis (Figure 3f). The DF image reveals yet a third incoherent domain (inset, Figure 3e) similar in size to the domains in Figure 3a–c. HRTEM and diffraction indicate that such a region is amorphous (Figure 3g). Thus, the nanoscale incoherent domains in Figure 3a,b may have been amorphized

during cycling, a pathway previously observed through in situ X-ray diffraction.[39,40] Even if the domain is crystalline, as in Figure 3c, it may have amorphized and recrystallized into a different crystal orientation during a previous cycle, consistent with the observations of Meethong et al.[39] and Kao et al.[40] Further experimental work is needed to confirm the extent of amorphization in LiFePO$_4$ particles during cycling.

Summarizing our experimental observations, we conducted SOC mapping on two partially discharged electrodes: one with 20 wt% carbon black (C20) and the other with 5 wt% carbon black (C5). In the C20 electrode, smaller particles lithiate before larger ones. In the C5 electrode, on the other hand, the size dependence is very weak. Additionally, the C20 electrode
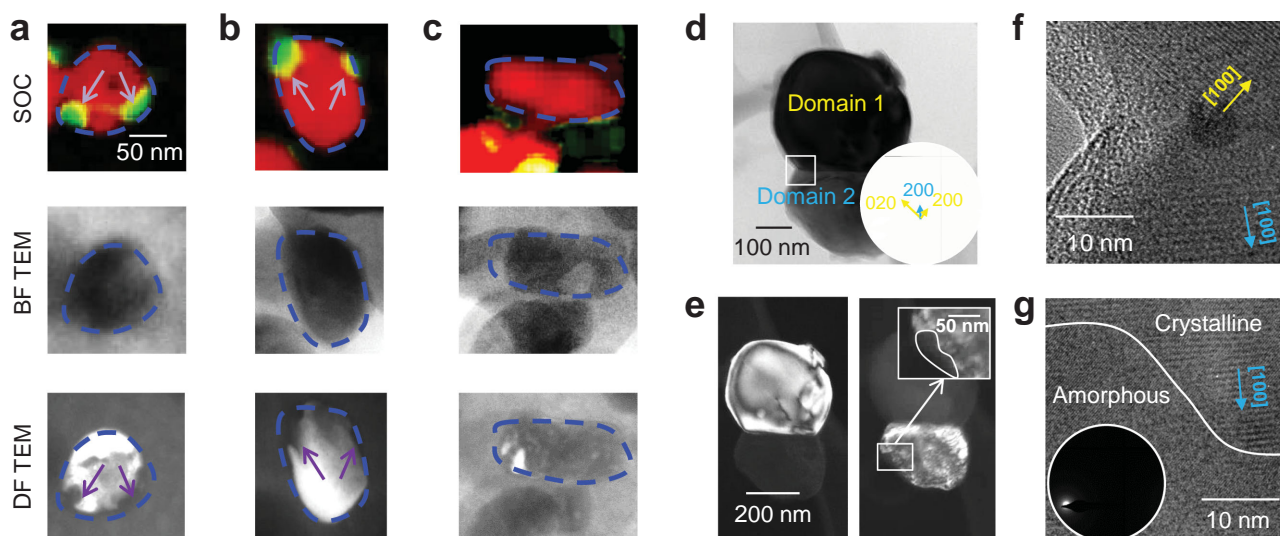
Figure 3. SOC maps and TEM images of crystallographically incoherent domains. a–c) SOC maps (from ptychography), bright field, and dark field TEM images of representative particles, revealing incoherent domains in the C20 electrode. In some particles, the lithiation front ends at the incoherent domains, marked by purple arrows in (a,b). The particles in (a–c) are circled in Figure 1c. The hue and brightness in the SOC maps have the same meaning as in Figure 1a–d. d) Bright field and diffraction of a particle from a cycled electrode. e,f) Dark field and HRTEM reveal two large incoherent crystal domains. The inset in (e) reveals a third smaller incoherent domain (marked in white). g) HRTEM and diffraction of the inset in (e) reveal an amorphous region of the particle, suggesting that the incoherent domains in (a–c) may have amorphized during cycling.
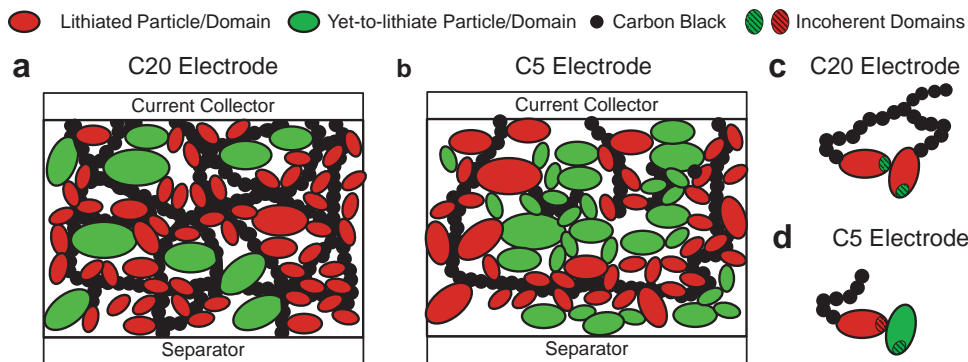
Figure 4. Scheme of the sequence of lithiation for a partially discharged electrode. a) Strong percolation of the carbon network in the C20 electrode causes smaller particles to preferentially lithiate due to increased surface area to volume ratios. b) In the C5 electrode, the better-connected particles closer to the carbon network with a direct connection to the current collector lithiate first, masking the size dependence. c) In the C20 electrode, the unconnected incoherent domains lithiate after the connected primary domain. d) In the C5 electrode, where certain particles have poor connectivity, the incoherent domains within well-connected particles lithiate before poorly connected particles.

contains some Li-rich particles with nanosized Li-poor domains. These Li-poor domains correspond to crystallographically incoherent, possibly amorphous, domains.

We propose that differences in the sequence of lithiation between the C5 and C20 electrodes arise due to the differing degrees of local electronic connectivity. Awarke et al. conducted a percolation-tunneling model of electrodes containing LiFePO$_4$ and carbon black, and showed that, for 200 nm spherical LiFePO$_4$ particles, the carbon black loading must be greater than 10 wt% to achieve critical electronic percolation (assuming that the LiFePO$_4$ particles are nonconducting).[34] Since the carbon black loading in the C20 electrode (20 wt%) is significantly above the percolation threshold, most of the carbon black particles belong to the largest, percolated cluster.[41] Additionally, due to the differences in the size between LiFePO$_4$ (≈230 nm, Figure S3, Supporting Information) and carbon black particles (≈50 nm, Figure S9, Supporting Information), the larger LiFePO$_4$ particles are presumably connected to at least one carbon black particle. As a result, the electronic connectivity of each particle to the carbon black network is relatively homogeneous, and the intrinsic preference for smaller particles to lithiate first is revealed (**Figure 4**a). We did not analyze the spatial distribution of the carbon black directly because our 2D cross-sections preclude a quantitative analysis of the 3D carbon black network.

The observation that smaller particles lithiate first could arise from three origins: a smaller nucleation barrier, faster ionic diffusion in smaller particles, or higher surface area to volume ratio. We first consider the nucleation barrier (or, more generally, the barrier arising from the non-monotonic chemical potential of Li in LiFePO$_4$[42]): while the barrier height depends on the particle size, its effects are pronounced only for particles smaller than 50 nm.[30,32,43] An overwhelming majority of particles in this study (97%) are larger than 100 nm (Figure S3, Supporting Information), making it unlikely that the nucleation barrier differs significantly among the particles. Next, we consider the case that larger particles may be Li-diffusion limited, slowing the rate of intercalation. Using a diffusivity of 10^{-8} cm s^{-1},[44] the estimated Li diffusion time for a large 500 nm particle is 0.25 s, significantly less than the electrode discharge time of 30 min. Additionally, in the solid-diffusion-limited

regime, the particles would lithiate concurrently,[45] in contrast to the particle-by-particle-like intercalation observed here. This leaves a surface-limited reaction[24] as the most likely explanation for the observed size dependence. That is, smaller particles have higher surface area to volume ratios and lithiate before the larger particles. Under both the single-phase solid solution and two-phase nucleation and growth pathways, the chemical potential of Li in LiFePO$_4$ decreases once the particles lithiate past the barrier,[14,42,46] estimated to be less than 20% lithiation fraction.[14,23] As a result, the smaller particles that lithiate to the barrier first would completely lithiate, even before the larger particles lithiate to the barrier. Thus, due to differences in surface area to volume ratios, we observe a mosaic of Li-rich small particles and Li-poor large particles.

In contrast to the C20 electrode, the sequence of lithiation in the C5 electrode depends weakly on the particle size. Since the C5 electrode contains 5 wt% carbon black, below the percolation threshold,[34] only some of the particles are directly connected to the current collector through the carbon black particles. LiFePO$_4$ particles with this direct connection would preferentially lithiate, largely independent of the particles' size (Figure 4b). Other LiFePO$_4$ particles may not rest adjacent to a carbon black particle, or the neighboring carbon black particle may not be directly connected to the current collector. In the absence of a direct electronic connection to the current collector, the amorphous carbon coating of LiFePO$_4$ particles provides another source of electronic conduction in the electrode; at ≈2 nm thick,[9] however, this thin coating is significantly more resistive than the ≈50 nm carbon black particles (Figure S9, Supporting Information). This heterogeneity in electronic connectivity suppresses the particle size dependence in the C5 electrode. Additionally, this variation in the electronic connectivity exists on a local (i.e., between a LiFePO$_4$ and a carbon black particle) rather than global (i.e., the distance from the LiFePO$_4$ particle to the current collector) level. This explains why there is no strong lithiation front from the current collector to the separator (Figure S7, Supporting Information). The resistive particle connectivity to the carbon black network also results in increased overpotential of the C5 electrode (Figure S2, Supporting Information), which was shown to be Ohmic.[14] We also consider the possibility that the higher carbon loading in

ADVANCED
MATERIALS
www.advmat.de

Materials
Views
www.MaterialsViews.com

COMMUNICATION

the C20 electrode may promote interparticle Li redistribution during or after coin cell disassembly because carbon black may conduct both Li^+ and e^-. However, significant interparticle redistribution would reduce the active particle population to near 0%, whereas the experimentally observed active particle populations of the two electrodes are nearly identical (14% and 12%). Finally, we note that, if two particles have similar electronic connectivity, the smaller one will lithiate first, reflecting differences in the surface area to volume ratios and explaining the weak size dependence observed in Figure 2b.

Our work definitively reconciles different experimental observations on the particle size dependence of lithiation. When the carbon black loading is high, as in ref. [10], the smaller particles preferentially lithiate, which likely reflects the difference in surface area to volume ratios. When the carbon black loading is low, the sequence of lithiation does not depend strongly on the particle size (e.g., as observed in ref. [9]). Our results experimentally validate models which show smaller particles lithiate before larger ones when the electronic connectivity is uniform.[14,22,33] Moreover, under technologically relevant carbon loading conditions, the local electronic connectivity of $LiFePO_4$ to the carbon network, as opposed to the particles' size or their distance from the current collector, determines the sequence of lithiation in $LiFePO_4$ electrodes. Thus, the local electronic transport between $LiFePO_4$ and the carbon black network is the most resistive process, even though the particles are carbon coated. To improve the rate capability without substantially decreasing the active material loading, a recent result shows that the critical percolation threshold is reduced to 1.5 wt% by using graphene nanosheets instead of carbon black.[47] A conductive mesoporous architecture with micronsized secondary particles[48–50] may also reduce the carbon black needed to achieve critical percolation.

Our results also have implications for porous electrode modeling, which typically only account for macroscopic electrode transport rather than local inhomogeneities in particle wiring.[45,51–54] The rate-limiting process in an electrode is typically assumed to be ion diffusion in the liquid electrolyte, ion diffusion in the solid active particles, and/or interfacial charge transfer between the particles and the electrolyte.[52] Here, we show that the local electron transport between the particles and the carbon black network is rate limiting. Because this effect is not typically accounted for, it is often difficult to fit porous electrode models to experimental voltage profiles. Additionally, because wiring resistances can be significant, it is essential to use electrodes with high carbon black loading in conducting fundamental electrochemical studies. This minimizes the convolution of interparticle electronic resistance in experimental current–voltage profiles.

Finally, our observation that lithiation stops abruptly at an incoherent domain boundary within a given particle in the C20 but not the C5 electrode can also be interpreted in terms of the local electronic wiring. Because the Li conduction channels in $LiFePO_4$ are 1D, Li cannot readily migrate from one domain to the next if the domains are crystallographically incoherent and the channels are misaligned. As a result, incoherent domains within a single particle can behave as isolated "particles." In the C20 electrode, we observe that many incoherent domains are delithiated (Figure 1c and 3a,b), so the incoherent domains are

generally the last to lithiate. We propose that, as the domain size decreases to below the size of a carbon black particle, the likelihood of being directly connected to the carbon network decreases. Instead, electrons conduct through the amorphous carbon coating on the particle. Accordingly, the nanoscale incoherent domains with poor access to carbon black particles are the last to lithiate (Figure 4c). In the C5 electrode, on the other hand, the heterogeneity in the connectivity between different particles overwhelms the heterogeneity between different domains within a particle (Figure 4d). Therefore, the incoherent domains lithiate at the same time as the remainder of a given particle. Because the phase diagram of $LiFePO_4$ is dependent on particle size when the particles are smaller than 50 nm,[30,32,43] thermodynamic factors may also play a role in the lithiation pathway of the small domains. It is also possible that Li redistributes between different domains in a particle after the electrode was disassembled, but the misalignment of the 1D diffusion channels across incoherent crystallite domains renders this unlikely. Similar to the particle size dependence of lithiation at the single-particle level, the intrinsic behavior of the nanoscale domains is again revealed through increased carbon connectivity.

In conclusion, we used high-resolution X-ray microscopy and correlative TEM to map the nanoscale SOC and determine the sequence of lithiation in a partially discharged $LiFePO_4$ electrode. For an electrode with high carbon black loading, smaller particles lithiate before larger ones due to increased surface area to volume ratios. For a more technologically relevant electrode with lower carbon black and higher active material loading, this size dependence is largely suppressed. We conclude that local electronic connectivity between a particle and the carbon network controls the lithiation pathway. Our work shows that understanding the sequence of lithiation can directly reveal loss mechanisms and rate-limiting processes in battery electrodes, and rationally guide the design and fabrication of electrode architectures with high power density.

Supporting Information

Supporting Information is available from the Wiley Online Library or from the author.

Acknowledgements

[1] A. K. Padhi, K. S. Nanjundaswamy, J. B. Goodenough, *J. Electrochem. Soc.* **1997**, *144*, 1188.

[2] M. Tang, W. C. Carter, Y.-M. Chiang, *Annu. Rev. Mater. Res.* **2010**, *40*, 501.

[3] C. Villevieille, M. Ebner, J. L. Gómez-Cámer, F. Marone, P. Novák, V. Wood, *Adv. Mater.* **2015**, *27*, 1676.

[4] F. Wang, L. Wu, B. Key, X. Q. Yang, C. P. Grey, Y. Zhu, J. Graetz, *Adv. Energy Mater.* **2013**, *3*, 1324.

[5] C. T. Campbell, S. C. Parker, D. E. Starr, *Science* **2002**, *298*, 811.

[6] A. Baldi, T. C. Narayan, A. L. Koh, J. A. Dionne, *Nat. Mater.* **2014**, *13*, 1143.

[7] J. P. Strachan, M. D. Pickett, J. J. Yang, S. Aloni, A. L. David Kilcoyne, G. Medeiros-Ribeiro, R. Stanley Williams, *Adv. Mater.* **2010**, *22*, 3573.

[8] G. Brunetti, D. Robert, J. L. Rouvi, E. F. Rauch, J. F. Martin, J. F. Colin, *Chem. Mater.* **2011**, *23*, 4515.

[9] W. C. Chueh, F. El Gabaly, J. D. Sugar, N. C. Bartelt, A. H. McDaniel, K. R. Fenton, K. R. Zavadil, T. Tyliszczak, W. Lai, K. F. McCarty, *Nano Lett.* **2013**, *13*, 866.

[10] D. Robert, T. Douillard, A. Boulineau, G. Brunetti, P. Nowakowski, D. Venet, P. Bayle-Guillemaud, C. Cayron, *ACS Nano* **2013**, *7*, 10887.

[11] U. Boesenberg, F. Meirer, Y. Liu, A. K. Shukla, R. Dell'anna, T. Tyliszczak, G. Chen, J. C. Andrews, T. J. Richardson, R. Kostecki, J. Cabana, *Chem. Mater.* **2013**, *25*, 1664.

[12] J. D. Sugar, F. El Gabaly, W. C. Chueh, K. R. Fenton, T. Tyliszczak, P. G. Kotula, N. C. Bartelt, *J. Power Sources* **2014**, *246*, 512.

[13] D. A. Shapiro, Y.-S. Yu, T. Tyliszczak, J. Cabana, R. Celestre, W. Chao, K. Kaznatcheev, A. L. D. Kilcoyne, F. Maia, S. Marchesini, Y. S. Meng, T. Warwick, L. L. Yang, H. A. Padmore, *Nat. Photonics* **2014**, *8*, 765.

[14] Y. Li, F. El Gabaly, T. R. Ferguson, R. B. Smith, N. C. Bartelt, J. D. Sugar, K. R. Fenton, D. A. Cogswell, A. L. D. Kilcoyne, T. Tyliszczak, M. Z. Bazant, W. C. Chueh, *Nat. Mater.* **2014**, *13*, 1149.

[15] J. Liu, M. Kunz, K. Chen, N. Tamura, T. J. Richardson, *J. Phys. Chem. Lett.* **2010**, *1*, 2120.

[16] F. C. Strobridge, B. Orvananos, M. Croft, H.-C. Yu, R. Robert, H. Liu, Z. Zhong, T. Connolley, M. Drakopoulos, K. Thornton, C. P. Grey, *Chem. Mater.* **2015**, *27*, 2274.

[17] Y. Li, J. Nelson Weker, W. E. Gent, D. N. Mueller, J. Lim, D. A. Cogswell, T. Tyliszczak, W. C. Chueh, *Adv. Funct. Mater.* **2015**, *25*, 3677.

[18] Y.-S. Yu, C. Kim, D. A. Shapiro, M. Farmand, D. Qian, T. Tyliszczak, A. L. D. Kilcoyne, R. Celestre, S. Marchesini, J. Joseph, P. Denes, T. Warwick, F. C. Strobridge, C. P. Grey, H. Padmore, Y. S. Meng, R. Kostecki, J. Cabana, *Nano Lett.* **2015**, *15*, 4282.

[19] W. H. Woodford, W. C. Carter, Y.-M. Chiang, *Energy Environ. Sci.* **2012**, *5*, 8014.

[20] M. Gaberscek, M. Küzma, J. Jamnik, *Phys. Chem. Chem. Phys.* **2007**, *9*, 1815.

[21] C. Fongy, S. Jouanneau, D. Guyomard, J. C. Badot, B. Lestriez, *J. Electrochem. Soc.* **2010**, *157*, A1347.

[22] B. Orvananos, R. Malik, H.-C. Yu, R. Malik, A. Abdellahi, C. P. Grey, G. Ceder, K. Thornton, *Electrochim. Acta* **2014**, *137*, 245.

[23] P. Bai, D. A. Cogswell, M. Z. Bazant, *Nano Lett.* **2011**, *11*, 4890.

[24] M. Z. Bazant, *Acc. Chem. Res.* **2013**, *46*, 1144.

[25] P. Bai, M. Z. Bazant, *Nat. Commun.* **2014**, *5*, 3585.

[26] R. Malik, F. Zhou, G. Ceder, *Nat. Mater.* **2011**, *10*, 587.

[27] M. Gaberscek, R. Dominko, J. Jamnik, *Electrochem. Commun.* **2007**, *9*, 2778.

[28] R. Malik, D. Burch, M. Bazant, G. Ceder, *Nano Lett.* **2010**, *10*, 4123.

[29] N. Meethong, H.-Y. S. Huang, W. C. Carter, Y.-M. Chiang, *Electrochem. Solid-State Lett.* **2007**, *10*, A134.

[30] M. Wagemaker, D. P. Singh, W. J. H. Borghols, U. Lafont, L. Haverkate, V. K. Peterson, F. M. Mulder, *J. Am. Chem. Soc.* **2011**, *133*, 10222.

[31] A. van der Ven, M. Wagemaker, *Electrochem. Commun.* **2009**, *11*, 881.

[32] D. A. Cogswell, M. Z. Bazant, *Nano Lett.* **2013**, *13*, 3036.

[33] T. R. Ferguson, M. Z. Bazant, *Electrochim. Acta* **2014**, *146*, 89.

[34] A. Awarke, S. Lauer, S. Pischinger, M. Wittler, *J. Power Sources* **2011**, *196*, 405.

[35] A. L. D. Kilcoyne, T. Tyliszczak, W. F. Steele, S. Fakra, P. Hitchcock, K. Franck, E. Anderson, B. Harteneck, E. G. Rightor, G. E. Mitchell, A. P. Hitchcock, L. Yang, T. Warwick, H. Ade, *J. Synchrotron Radiat.* **2003**, *10*, 125.

[36] H. Bluhm, K. Andersson, T. Araki, K. Benzerara, G. E. Brown, J. J. Dynes, S. Ghosal, M. K. Gilles, H.-C. Hansen, J. C. Hemminger, A. P. Hitchcock, G. Ketteler, A. L. D. Kilcoyne, E. Kneedler, J. R. Lawrence, G. G. Leppard, J. Majzlam, B. S. Mun, S. C. B. Myneni, A. Nilsson, H. Ogasawara, D. F. Ogletree, K. Pecher, M. Salmeron, D. K. Shuh, B. Tonner, T. Tyliszczak, T. Warwick, T. H. Yoon, *J. Electron Spectrosc. Relat. Phenom.* **2006**, *150*, 86.

[37] P. Thibault, M. Dierolf, A. Menzel, O. Bunk, C. David, F. Pfeiffer, *Science* **2008**, *321*, 379.

[38] X. Liu, J. Liu, R. Qiao, Y. Yu, H. Li, L. Suo, Y. Hu, Y.-D. Chuang, G. Shu, F. Chou, T.-C. Weng, D. Nordlund, D. Sokaras, Y. J. Wang, H. Lin, B. Barbiellini, A. Bansil, S. Xiangyun, Z. Liu, S. Yan, G. Liu, S. Qian, T. J. Richardson, D. Pendergast, H. Zahid, F. M. F. de Groot, W. Yang, *J. Am. Chem. Soc.* **2012**, *134*, 13708.

[39] N. Meethong, Y. Kao, M. Tang, H. Huang, W. C. Carter, Y. Chiang, *Chem. Mater.* **2008**, *4*, 6189.

[40] Y. Kao, M. Tang, N. Meethong, J. Bai, W. C. Carter, Y.-M. Chiang, *Chem. Mater.* **2010**, *22*, 5845.

[41] D. Stauffer, A. Aharony, *Introduction to Percolation Theory*, Taylor & Francis Group, London, UK **1994**.

[42] W. Dreyer, J. Jamnik, C. Guhlke, R. Huth, J. Moskon, M. Gaberscek, *Nat. Mater.* **2010**, *9*, 448.

[43] A. Abdellahi, O. Akyildiz, R. Malik, K. Thornton, G. Ceder, *J. Mater. Chem. A* **2014**, *2*, 15437.

[44] D. Morgan, A. Van der Ven, G. Ceder, *Electrochem. Solid-State Lett.* **2004**, *7*, A30.

[45] T. R. Ferguson, M. Z. Bazant, *J. Electrochem. Soc.* **2012**, *159*, A1967.

[46] R. Malik, A. Abdellahi, G. Ceder, *J. Electrochem. Soc.* **2013**, *160*, A3179.

[47] B. Zhang, Y. Yu, Y. Liu, Z.-D. Huang, Y. He, J.-K. Kim, *Nanoscale* **2013**, *5*, 2100.

[48] J. Qian, M. Zhou, Y. Cao, X. Ai, H. Yang, *J. Phys. Chem. C* **2010**, *114*, 3477.

[49] G. Wang, H. Liu, J. Liu, S. Qiao, G. M. Lu, P. Munroe, H. Ahn, *Adv. Mater.* **2010**, *22*, 4944.

[50] C. Sun, S. Rajasekhara, J. B. Goodenough, F. Zhou, *J. Am. Chem. Soc.* **2011**, *133*, 2132.

[51] J. Newman, K. E. Thomas-Alyea, *Electrochemical Systems*, Prentice Hall, Eglewood Cliffs, NJ **2004**.

[52] V. Srinivasan, J. Newman, *J. Electrochem. Soc.* **2004**, *151*, A1517.

[53] V. Srinivasan, J. Newman, *Electrochem. Solid-State Lett.* **2006**, *9*, A110.

[54] S. Dargaville, T. W. Farrell, *J. Electrochem. Soc.* **2010**, *157*, A830.